



High activity of Pt–Rh supported on C–ITO for ethanol oxidation in alkaline medium

V. F. de Carmargo¹ · E. H. Fontes¹ · J. Nandenha¹ · R. F. B. de Souza¹ · A. O. Neto¹

Received: 31 July 2019 / Accepted: 24 November 2019 / Published online: 18 December 2019
© Springer Nature B.V. 2019

Abstract

PtRh/C–ITO electrocatalysts were prepared in a single-step method using $\text{H}_2\text{PtCl}_6 \cdot 6\text{H}_2\text{O}$ and $\text{RhCl}_3 \cdot x\text{H}_2\text{O}$ as metal sources, sodium borohydride as the reducing agent and a physical mixture of 85% Vulcan Carbon XC72 and 15% $\text{In}_2\text{O}_3 \cdot \text{SnO}_2$ (indium tin oxide—ITO) as support. PtRh/C–ITO were characterized by X-ray diffraction, transmission electron microscopy, X-ray photoelectron spectroscopy (XPS), cyclic voltammetry, chronoamperometry, attenuated total reflectance, Fourier transform infrared spectroscopy and performance test on direct alkaline ethanol fuel cell. X-ray diffraction patterns for all PtRh/C–ITO indicated a shift in Pt (fcc) peaks, showing that Rh was incorporated into Pt lattice. Transmission electron microscopy for PtRh/C–ITO showed nanoparticles homogeneously distributed over the support with particles size between 3.0 and 4.0 nm. The XPS results for Pt70Rh30/C–ITO showed the presence of mixed oxidation states of Sn^0 and SnO_2 that could favor the oxidation of adsorbed intermediates by bifunctional mechanism. Pt90Rh10/C–ITO was more active in electrochemical studies, which could be associated with the C–C bond break. Experiments in direct alkaline ethanol fuel cells showed that the power density values obtained for Pt70Rh30/C–ITO and Pt90Rh10/C–ITO were higher than Pt/C, indicating the beneficial effect of Rh addition to Pt and the use of C–ITO support.

Keywords Sodium borohydride reduction process · PtRh/C–ITO electrocatalysts · Ethanol oxidation · In situ ATR-FTIR, alkaline electrolytes · Polarization curves

✉ A. O. Neto
aolivei@ipen.br

¹ Instituto de Pesquisas Energéticas e Nucleares, IPEN/CNEN-SP, Av. Prof. Lineu Prestes, 2242
Cidade Universitária, São Paulo, SP CEP 05508-000, Brazil

Introduction

A combination of Pt-based bimetallic nanoparticles (PtSn, PtNi, PtRh, PtPd, etc.) has been studied for ethanol oxidation reaction (EOR), where the enhanced of activity is usually attributed to the bifunctional mechanism or synergistic effect. PtRh supported on carbon have been more employed more and more as electrocatalysts for direct ethanol fuel cell, because of their high catalytic activities and the ability of efficient C–C bond cleavage [1–8]. Adzic [9] showed that the rhodium sites are able to adsorb ethanol in alkaline medium, therefore this ability being interesting for fuel cell applications in this medium.

Fontes et al. [10] showed that PtRh/C 50:50 prepared by sodium borohydride method were more active for ethanol oxidation in alkaline medium in comparison with Pt/C and Rh/C. The best activity of PtRh/C 50:50 was attributed to the CO₂ production that coincides with the decrease in the signal of acetate and carbonate ions observed in situ ATR-FTIR experiments.

Souza et al. [11] showed that a PtRh/C (70:30) prepared by an alcohol reduction process were more active than Pt/C and Rh/C for ethanol oxidation in alkaline medium. The best activity of PtRh/C (70:30) was due to the smaller quantities of carbonate ions produced and the production of higher quantities acetate ions, when compared to the other electrocatalysts prepared.

Liu et al. [12] showed that core sheath Rh@Pt electrocatalysts have an enhanced activity and greater durability for ethanol oxidation in an acidic medium; this behavior was attributed to an enhanced interaction between Pt layer and the Rh nanowire, which can promote C–C bond cleavage to CO₂, while depress the dehydrogenation of ethanol to acetic acid.

Shen et al. [13] showed that Pt₂Rh/C electrocatalysts prepared by the microwave–polyol method had a higher catalytic activity for ethanol oxidation in alkaline media in terms of the onset potential and the peak current density in comparison with Pt/C. This behavior was associated with the improvement of the C–C bond cleavage in the presence of Rh, as the acceleration kinetics in an alkaline medium.

Another route would be to use of Pt electrocatalysts decorated with metal oxides such as TiO₂, SnO₂, RuO₂, Sb₂O₅·SnO₂ (ATO), In₂O₃, In₂O₃·SnO₂ (ITO) and CeO₂. These materials significantly enhance the catalytic activity and electrochemical stability for ethanol oxidation. The presence of these metal oxides on carbon support may also improve the corrosion resistance but, at the same time, hinder the electrochemical active surface area [14–22].

Eguiluz et al. [23] showed that PtRh nanowires supported on Sb₂O₅·SnO₂ nanoparticles have a lower onset potential and a greater resistance to poisoning by intermediate species. This behavior could be attributed to the presence of carbon ATO used as support, and the provision of OH species by ATO itself, facilitating the oxidation of ethanol at a lower potential, and modified the lattice parameter of Pt.

Pereira et al. [24] showed that PtSn/C–In₂O₃·SnO₂ had superior performance for ethanol oxidation in alkaline or acid electrolytes. The high activity was attributed to bifunctional mechanism, electronic effect and the synergetic interaction between PtSn nanoparticles and In₂O₃·SnO₂-C used as support.

In this context, PtRh/C–In₂O₃·SnO₂ electrocatalysts were prepared for the first time by the borohydride reduction process [25] in different Pt/Rh atomic ratios for ethanol oxidation in alkaline electrolytes. In this work are included structural analysis, electrochemical experiments, in situ ATR-FTIR studies for obtaining information about products formed for ethanol oxidation and single-ethanol fuel cell.

Experimental

PtRh/C–In₂O₃·SnO₂ electrocatalysts (20% of metal loading, with Pt/Rh atomic ratios of 100:0, 90:10, 70:30, 50:50 and 0:100 and with C/In₂O₃·SnO₂ mass ratios of 100:0 and 85:15) were prepared using H₂PtCl₆·6H₂O (chloroplatinic acid—Aldrich) and RhCl₃·xH₂O (rhodium chloride—Aldrich) as metal sources, sodium borohydride (Aldrich) as reducing agent and Vulcan Carbon XC72 (Cabot Corporation) and In₂O₃·SnO₂ (Aldrich) as support.

In the borohydride reduction process, the metal sources were dissolved in a mixture of water/2-propanol (50/50, v/v) and the Vulcan XC72 + In₂O₃·SnO₂ support was dispersed in the solution. The mixture obtained was treated with an ultrasonic bath for 10 min and was right after put back under magnetic stirring. The solution of sodium borohydride, containing 5 times the molar amount of metal sources (0.1025 mol L⁻¹ for Pt, 0.1076 mol L⁻¹ for Pt₉₀Rh₁₀, 0.1195 mol L⁻¹ for Pt₇₀Rh₃₀, 0.1342 mol L⁻¹ for Pt₅₀Rh₅₀ and 0.1944 mol L⁻¹ for Rh), was added at once at room temperature, and the mixture was let to stir for about 30 min. The stirring was stopped, and after 30 min the solids obtained from a simple filtration were water-washed and dried for 2 h at 70 °C.

X-ray powder diffraction (XRD) diagrams were obtained using a Rigaku diffractometer model Miniflex II, using K α source ($\lambda = 1.54,056 \text{ \AA}$) at $2\theta = 20^\circ$ to 90° with a step size of 0.05° and a scan time of 2 s per step. The morphology, distribution and size of nanoparticles were determined using a JEOL JEM-2100 LaB6 electron microscope operated at 200 kV. The sample was prepared by suspending 1 mg of the electrocatalysts on distilled water/isopropanol 50:50 sonicated for 15 min. After a small drop was put on the center of carbon-film grid using a micropipette and dried, the sample was inserted on TEM. About 200 particles from different regions were counted, for each sample, to determine the mean particle sizes.

X-ray photoelectron spectroscopy was done at LNNANO in CNPEM facility using the K-alpha (Thermo Scientific) X-ray photoelectron spectrometer. An aluminum source (Al $K\alpha$) with a 100–4000 eV electron gun was used. The vacuum pressure was reached with two 220 L s⁻¹ turbomolecular pumps, one for each input chamber and analysis chamber. Sample holder consisted of a four-axis stage with an area of 60 by 60 mm and max width of 20 mm. For the determination of the metallic elements and its oxidation states was used the concept of atomic sensitivity factor [26]. For this analysis was used the Origin software.

All cyclic voltammetry (CV) and chronoamperometry (CA) tests were performed on a Metrohm Autolab PGSTAT302N with a three-electrode cell. A Ag/AgCl in 3 mol L⁻¹ KCl was used as reference electrode, and the counter electrode was made of Pt. The composing of the working electrode (geometric area of 0.3 cm² with a

depth of 0.3 mm) follows the thin porous coating technique [24]. A mass of 10 mg of dry electrocatalyst and 100 μL of a PTFE solution (6 wt%) were added to a beaker containing 50 mL of DI water, which was after left in an ultrasonic bath for 5 min. The dispersed mixture was then filtered, and the obtained mass was inserted on the surface of the work electrode. The electrochemical measurements were realized in both aqueous KOH (1 mol L^{-1} KOH) and ethanol/KOH (1 mol L^{-1} EtOH/1 mol L^{-1} KOH) N_2 saturated solutions.

The spectro-electrochemical ATR-FTIR in situ measurements were performed with a Nicolet 6700 FT-IR spectrometer equipped with an MCT detector cooled with liquid N_2 , ATR accessory (MIRacle with a Diamond/ZnSe Crystal Plate Pike®). The working electrodes were the same as used in the electrochemical experiments in the presence of 1.0 mol L^{-1} ethanol + 1 mol L^{-1} KOH. Absorbance spectra were collected as the R/R_0 ratio, where R represents a spectrum at a given potential and R_0 is the spectrum collected at -0.85 V. Positive and negative directional bands represent gain and loss of species at the sampling potential, respectively. The spectra were computed from 128 interferograms averaged from 3000 to 850 cm^{-1} , with the spectral resolution set to 8 cm^{-1} . Initially, a reference spectrum (R_0) was measured at -0.85 V, and the sample spectra were collected after applying successive potential steps of 0.1 V until 0.05 V.

All anode and cathode electrodes were built with a load of 1 mg of metal per cm^2 , and all cathodes were made using commercial 20 wt% Pt/C (BASF) and all anodes using the prepared electrocatalysts in this study. All electrodes were prepared by painting the Nafion soaked catalyst ink, over a PTFE-treated carbon cloth, in a homogeneously dispersed fashion. The ink was previously prepared using the dry electrocatalysts and a Nafion solution (5 wt%, Aldrich). A Nafion 117 membrane, previously treated in a KOH solution, was placed between electrodes, and the assembly was hot pressed under a pressure of 247 kgf cm^{-2} for 3 min at 125 $^\circ\text{C}$. The fuel (ethanol 2.0 mol L^{-1} /3.0 mol L^{-1} KOH) was delivered at 1.0 mL min^{-1} , and the oxygen flow was regulated at 150 mL min^{-1} . Cell and O_2 humidifier temperatures were set, respectively, to 80 $^\circ\text{C}$ and 85 $^\circ\text{C}$. Polarization curves were obtained using a potentiostat/galvanostat PGSTAT302N Autolab.

Results and discussion

XRD patterns of PtRh/C are illustrated in Fig. 1. For all PtRh/C-ITO electrocatalysts were observed a peak at $2\theta=25^\circ$ associated with carbon structure (002) [24], four peaks at $2\theta=40^\circ$, 47° , 67° and 82° associated with the (111), (200), (220) and (311) planes, characteristic of face-centered cubic (fcc) structure of Pt and Pt alloys and peaks at about $2\theta=21^\circ$, 31° , 36° , 51° and 60° corresponding to the (221), (222), (400), (440) and (622) plane characteristics of In_2O_3 cubic structure [11, 24]. The diffraction peaks of PtRh/C-ITO were shifted to higher 2θ values compared to Pt/C electrocatalyst indicating a formation of PtRh alloys. The lattice parameter values obtained by the Pawley method [27, 28] carried out with Fityk 0.98 software for PtRh/C-ITO (90:10), PtRh/C-ITO (70:30) and PtRh/C-ITO (50:50) were 3.91 nm (67.9°)–3.96 nm (66.8°); 3.95 nm (67.0°)–3.88 nm (68.3°); and 3.96 nm

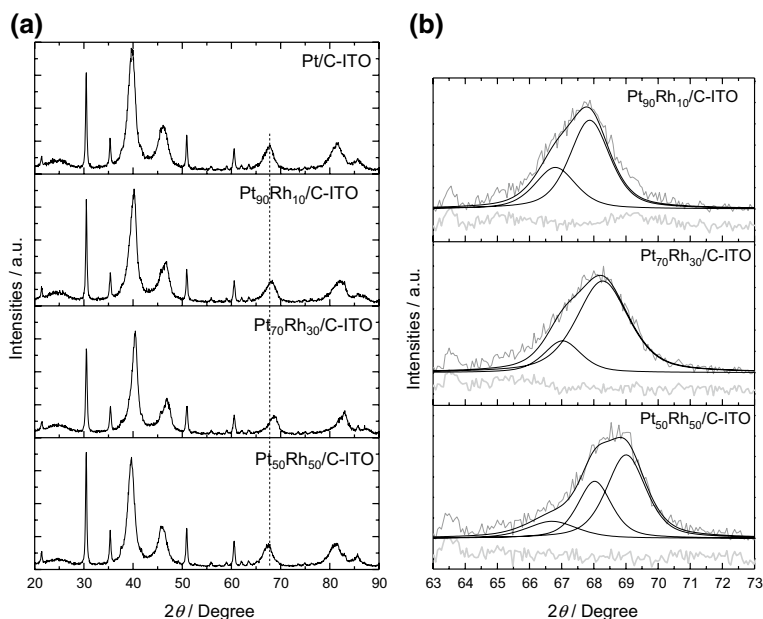


Fig. 1 **a** X-ray diffractograms of the Pt/C–ITO, Rh/C–ITO and PtRh/C–ITO electrocatalysts and **b** Pawley refinement gray for measured, black for modeled and light gray for residual line

(66.7°)–3.90 nm (68.0°)–3.84 (69.0°), where these values could be related to Pt (220) (JCPDF #04 802), Rh (220) (JCPDF #88 2334) and PtRh (220) [10].

Figure 2 illustrates TEM micrographs with the histograms of the particle size distribution for Pt/C–ITO, PtRh/C–ITO and Rh/C–ITO. All electrocatalysts prepared showed a good distribution of the nanoparticles on the support, and the morphologies are similar. For Pt/C–ITO, PtRh/C–ITO (90:10), PtRh/C–ITO (70:30), PtRh/C–ITO 50:50 and Rh/C–ITO was observed a mean diameter of the nanoparticles of 4.1 nm, 3.7 nm, 4.0 nm, 4.0 nm and 5.6 nm, respectively.

Figure 3 shows the XPS core-level spectra of C1 s in PtRh(90:10)/C–ITO, PtRh(70:30)/C–ITO and PtRh(50:50)/C–ITO. The peak center is about 284 eV for all materials, which is consistent with Moulder et al. [26]. For PtRh(50:50)/C–ITO one can notice a small shift for small values of B.E. compared to the other materials which can be caused by the dominant presence of C–C bonds over CO_x-type bonds in carbon structure of Carbon Vulcan XC72. We can also notice different In oxidation states: In₂O₃ for PtRh(50:50)/C–ITO and PtRh(70:30)/C–ITO and In₂O for PtRh(90:10)/C–ITO. These values of B.E. are also following Moulder et al. [26], and these differences in oxidation happen because In has different active sites' exposure to ambient oxygen depending on which metal is bonding to it.

The O1s peak is present for all materials studied and for PtRh(70:30)/C–ITO there is a small shift to higher values of B.E., which agrees with the broad peak of Sn3d for this same material. It is considered here that peak broadening is directly related to chemical shift effects. The O1s core-level spectra of PtRh(50:50)/C–ITO seem to be a result of a convolution of O1s present in PtRh(70:30)/C–ITO and

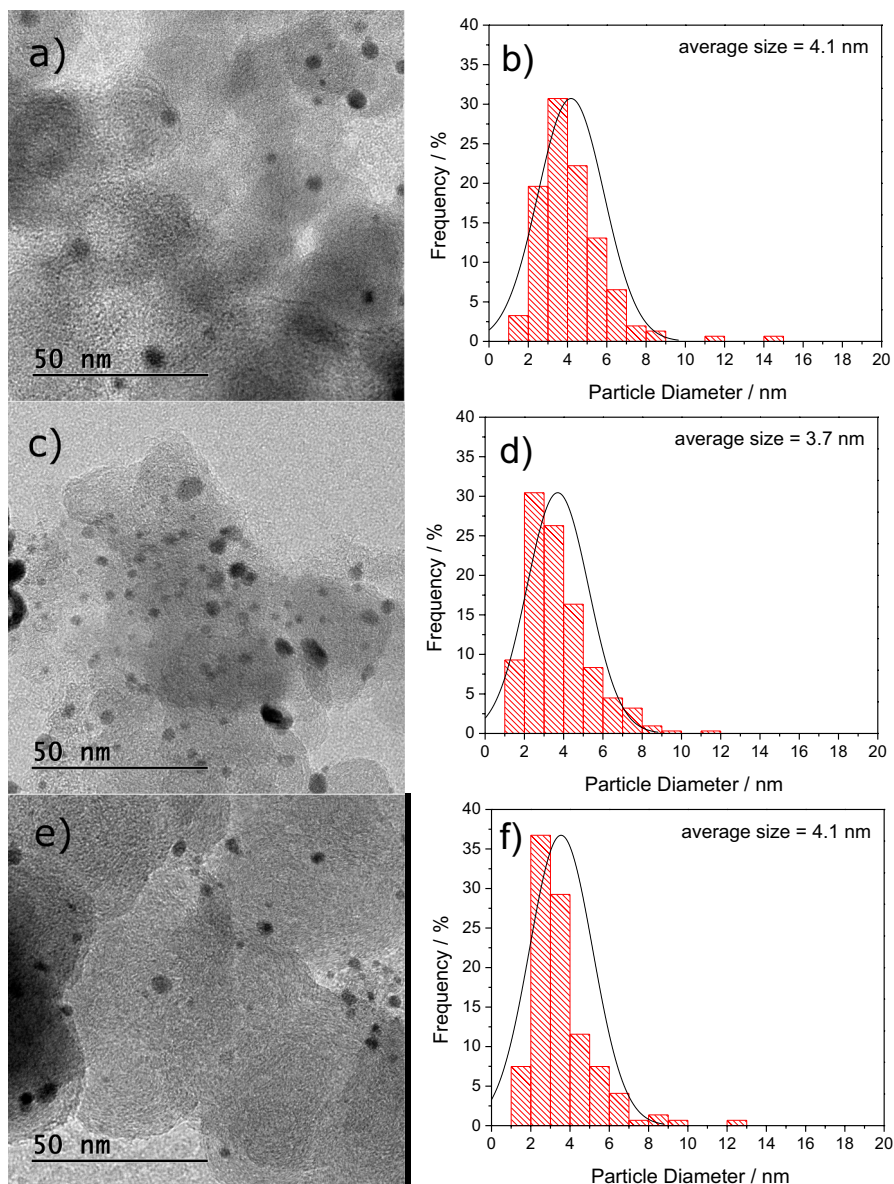


Fig. 2 **a** Micrograph Pt/C-ITO; **b** histogram Pt/C-ITO; **c** micrograph PtRh/C-ITO (90:10); **d** histogram PtRh/C-ITO (90:10); **e** micrograph PtRh/C-ITO (70:30); **f** histogram PtRh/C-ITO (70:30); **g** micrograph PtRh/C-ITO (50:50); **h** histogram PtRh/C-ITO (50:50); **i** micrograph Rh/C-ITO; **j** histogram Rh/C-ITO

PtRh(90:10)/C-ITO, because the amount of In, Sn, C, and O is essentially larger for PtRh(50:50)/C in surface compared to the other materials (this can be noticed qualitatively in the CPS intensity for all materials studied) [9, 26, 29].

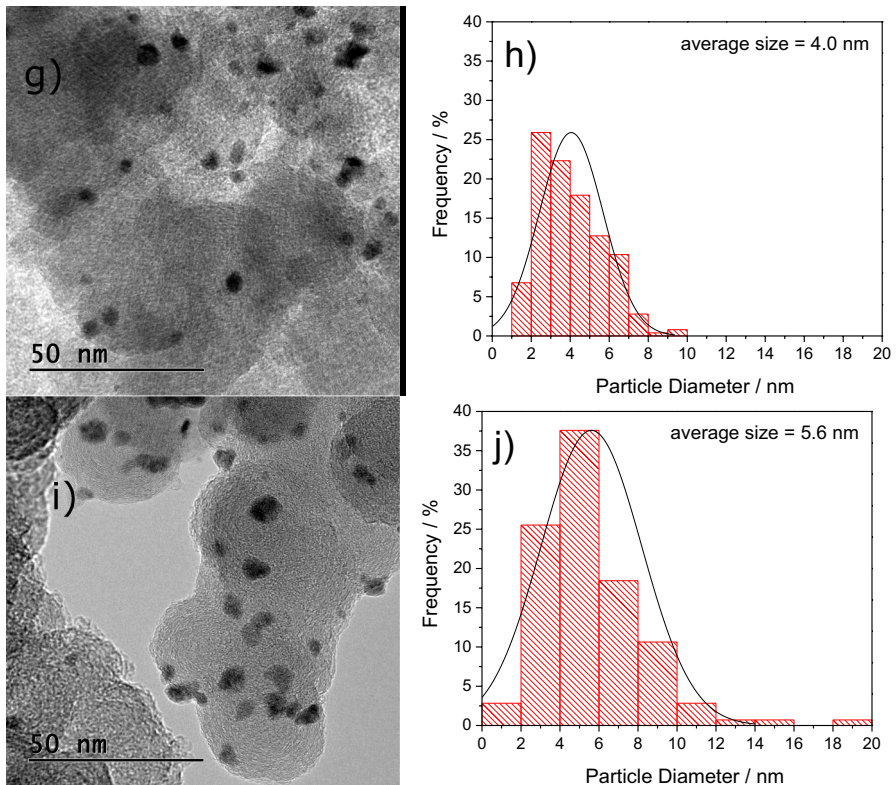


Fig. 2 (continued)

Sn3d for PtRh(70:30)/C–ITO peak is broader than the other materials because the presence of mixture states of Sn₀ and SnO₂ is more significant than the other materials. But it is worthy to mention again that the amount of In, Sn, C, and O for PtRh(50:50)/C–ITO is larger than the other materials [26].

Figure 4 shows the doublet states of the XPS core-level spectra of Pt4f for PtRh(90:10)/C–ITO, PtRh(70:30)/C–ITO and PtRh(50:50)/C–ITO. All the binding energies associated with the different oxidation species are in accordance with [26]. For all of them, it was seen only Pt⁰. It seems that the atomic oxygen was preferable to bond with the support C–ITO. It is noteworthy that Rh3d intensity band is linearly proportional with Rh content, while Pt is not. Pt4f intensity band for PtRh(50:50)/C–ITO is higher than Pt4f intensity band for PtRh(70:30)/C–ITO, and Pt4f for PtRh(90:10)/C has the higher intensity. This nonlinear proportionality may be attributed to the way of the reduction metal salts were reduced [25].

The largest amount of C, In, Sn, O and Rh in the surface of Pt50Rh50/C–ITO strongly supports the argument of bifunctional mechanism through this paper for this material. Although Pt4f of Pt50Rh50/C–ITO does not have the most intense doublet band, the large amount of C–ITO can play a decisive role concerning the

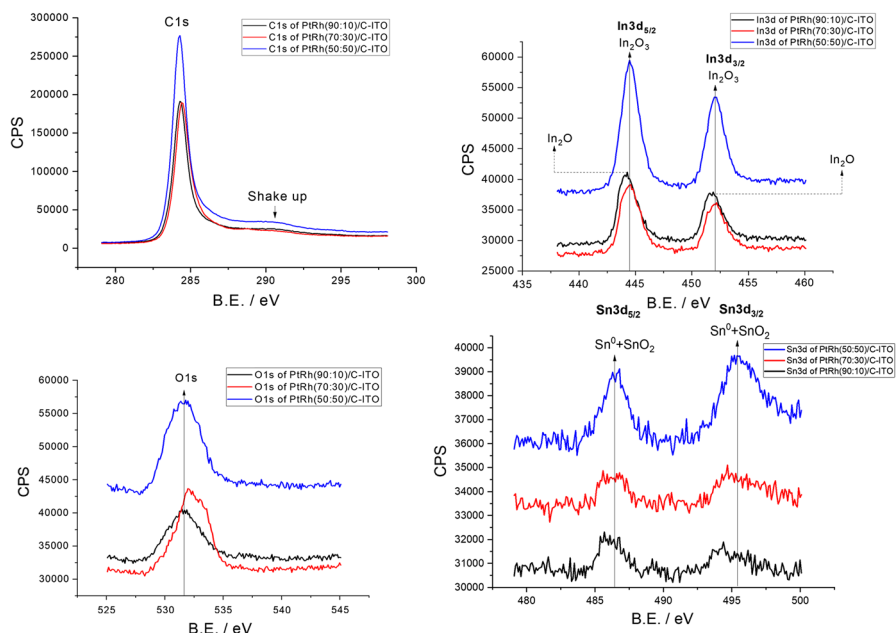


Fig. 3 Core-level XPS spectra of C 1 s, In 3d, O 1 s and Sn 3d of PtRh(90:10)/C–ITO, PtRh(50:50)/C–ITO and PtRh(70:30)/C–ITO

electrochemical activity through the bifunctional mechanism [25]. But the intensity of Pt 4f band for Pt90Rh10/C–ITO in the surface is almost 60% higher than Pt 4f of Pt70Rh30/C–ITO. Therefore, Pt90Rh10/C–ITO has the largest availability of Pt active sites when compared to the other ones, and because of that this electrocatalyst will present the better electrochemical activity. It is noteworthy to mention that this correlation can be done only for electrochemical experiments, since the electrode preparation for DEFC is different from the electrochemical experiments and other factors could influence the oxidation states observed in XPS experiment for DEFC electrocatalysts.

The cyclic voltammetry (CV) for Pt/C–ITO, Rh/C–ITO and PtRh/C–ITO electrocatalysts in the presence of 1 mol L⁻¹ KOH is illustrated in Fig. 5. PtRh/C–ITO, Pt/C–ITO and Rh/C–ITO electrocatalysts do not have a well-defined hydrogen adsorption–desorption region (–0.85 to –0.45 V) as observed for Pt/C electrocatalyst; this behavior may be associated with the presence of rhodium and ITO. Pt/C–ITO and all PtRh/C–ITO showed a peak in scan reverse between –0.3 and –0.4 V, which could be attributed to reduced PtO_x species. Also were observed in anodic scan a peak in –0.3 V related to the presence of ITO and a second peak in –0.1 V associated with the formation of Pt and Rh oxide species.

Figure 6 shows the cyclic voltammetry for ethanol oxidation using Pt/C–ITO, PtRh/C–ITO and Rh/C–ITO electrocatalyst obtained at a scan rate of 10 mV s⁻¹ between –0.85 and 0.2 V in 1.0 mol L⁻¹ of ethanol and 1.0 mol L⁻¹ KOH.

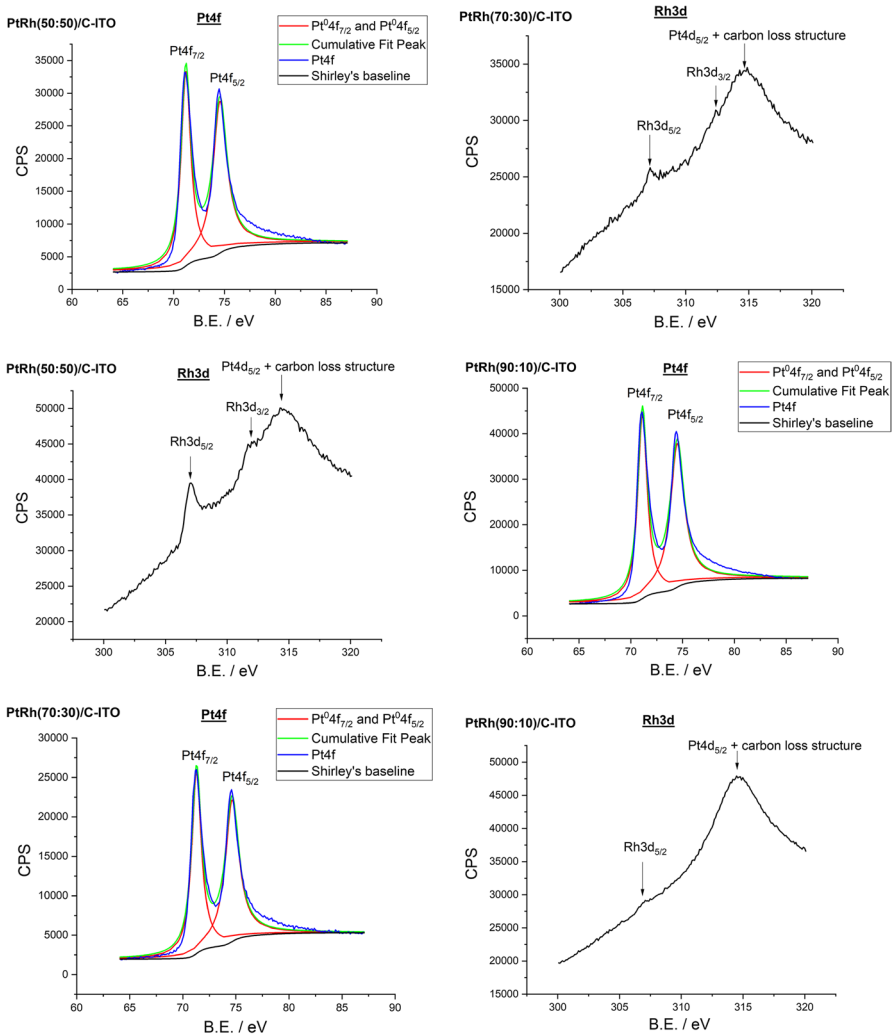


Fig. 4 Core-level XPS spectra of Pt4f and Rh3d of PtRh(90:10)/C–ITO, PtRh(50:50)/C–ITO and PtRh(70:30)/C–ITO

At first, one may notice that the onset potential value for the Rh/C–ITO (-0.65 V) was lower than the onset value of the other prepared electrocatalysts (-0.55 V). However, the rhodium electrocatalyst had the lowest current density within the potential range of -0.55 V and 0.2 V. One may also notice that PtRh/C–ITO and Pt/C–ITO electrocatalysts were more active than Pt/C at potentials above -0.6 V; many authors obtained similar results [13, 14, 30, 31].

Bai et al. [30] showed that the introduction of Rh to Pt was responsible for the low-onset oxidation potential of Pt1Rh1 in comparison with Pt/C; the current of Pt1Rh1 also was eight times higher than that at Pt nanocrystal electrocatalyst, so

Fig. 5 Cyclic voltammograms of Pt/C, PtC-ITO, Rh/C-ITO and PtRh/C-ITO electrocatalysts in 1 mol L⁻¹ KOH solution with a scan rate of 10 mV s⁻¹ at 25 °C

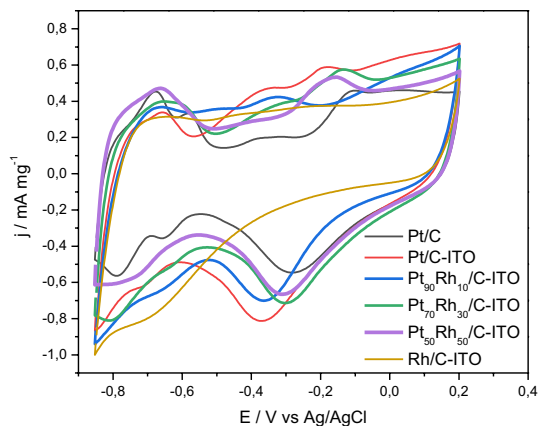
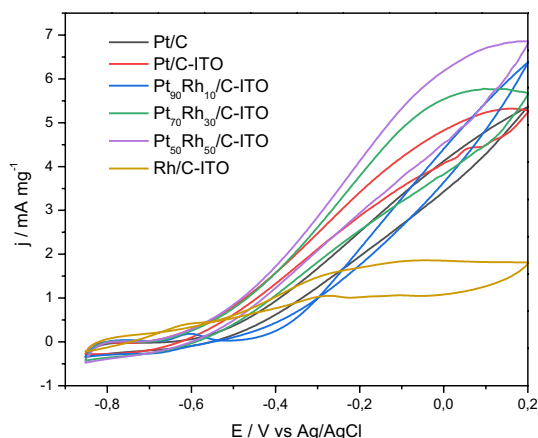


Fig. 6 Cyclic voltammograms of Pt/C-ITO, PtRh/C-ITO and Rh/C-ITO electrocatalyst in 1 mol L⁻¹ ethanol solution in 1.0 mol L⁻¹ KOH with a sweep rate of 10 mV s⁻¹



they concluded that the introduction of Rh was efficient at breaking C–C bonds, which is in high CO₂ selectivity.

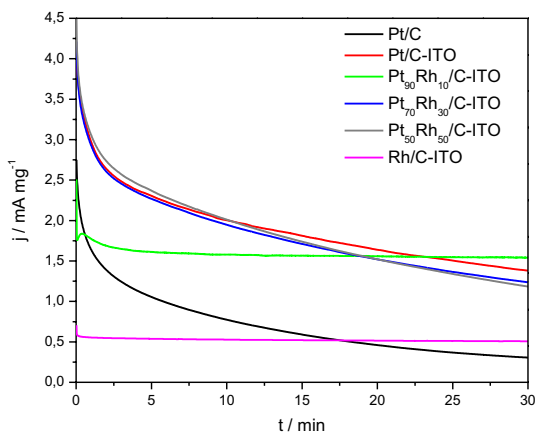
Wang et al. [14] showed that Pt₉Rh₁/TiO₂-C had the highest activity and stability when compared to Pt/C. The best activity was attributed to the presence of Rh and TiO₂, which facilitated the cleavage of C–C bond in ethanol and promoted low potential oxidation of intermediates.

Fang et al. [31] showed that Rh₅@Pt₅/C was 64% more active than on Pt₅/C, where the activity was attributed to the Rh core that enhanced the catalytic activity of the Pt shell, promoting the break of C–C bonds of ethanol.

Shen et al. [13] showed that a Pt₂Rh/C catalyst had a higher catalytic activity in comparison with Pt/C, where the enhanced activity was described by both an improvement in C–C bond cleavage and an accelerated oxidation kinetics of intermediate adsorbed in an alkaline medium.

The chronoamperometry results for Pt/C-ITO, Rh/C-ITO and PtRh/C-ITO electrocatalysts in the potential of –0.3 V for 30 min are illustrated in Fig. 7. For

Fig. 7 Current–time curves at -0.3 V in 1 mol L^{-1} ethanol solution in 1 mol L^{-1} KOH for Pt/C–ITO, Rh/C–ITO and PtRh/C–ITO electrocatalysts at 25°C



all prepared electrocatalysts, regarding their current density values, a fast decay was observed during the first minute. After a couple minutes, one may notice that Rh/C–ITO and Pt₉₀Rh₁₀/C–ITO had the lowest decay rate, while the other electrocatalysts had similar decay rates. After 20 min, the current density value of Pt/C is lower than Rh/C–ITO, which indicates its catalytic deactivation in a more significant way. Therefore, after this interval, Rh/C–ITO showed higher current values in comparison with Pt/C indicating its better activity for ethanol electro-oxidation in alkaline medium, which confirms the results of Adzic [9]. After 30 min, the final current density values at -0.3 V were: Pt₉₀Rh₁₀/C–ITO (1.5 A g^{-1}) > Pt/C–ITO (1.38 A g^{-1}) > Pt₇₀Rh₃₀/C–ITO (1.24 A g^{-1}) > Pt₅₀Rh₅₀/C–ITO (1.18 A g^{-1}) > Rh/C–ITO (0.50 A g^{-1}) > Pt/C (0.3 A g^{-1}). All obtained values are normalized by the weight of catalyst metals load. The high activity of Pt or PtRh electrocatalysts with $\text{In}_2\text{O}_3\cdot\text{SnO}_2\text{-C}$ used as support could be attributed to bifunctional mechanism, electronic effect and the synergistic interaction between nanoparticles and $\text{In}_2\text{O}_3\cdot\text{SnO}_2\text{-C}$ used as support.

Figure 8 shows the IR absorbance spectra obtained by in situ ATR-FTIR experiments in the region between 3000 and 850 cm^{-1} recorded during ethanol electro-oxidation in the function of the potential applied for Pt/C, Pt/C–ITO, PtRh/C–ITO (90:10), PtRh/C–ITO (70:30), PtRh/C–ITO (50:50) and Rh/C–ITO. For Pt/C, Pt/C–ITO and PtRh/C–ITO electrocatalyst was observed the presence of bands related to CO_2 , acetate, carbonate ions and acetaldehyde, while for Rh/C–ITO it was observed only bands related to carbonate ions. The bands of carbonate ion, acetate, acetaldehyde and CO_2 were observed at 1370 cm^{-1} [32], 1410 cm^{-1} [32], 926 cm^{-1} [33] and 2343 cm^{-1} [34], respectively; however, also it is possible to observe the presence of bands of consumption ethanol at 1080 , 1036 and 874 cm^{-1} [10]. These ethanol bands are negative in an absorbance spectrum, so they are associated with ethanol consumption [10].

The bands were deconvoluted to Lorentzian line shapes to better observe the product formation in the different potentials. These results are presented in Fig. 9. PtRh/C–ITO (70:30) and PtRh/C–ITO (90:10) showed intense formation of CO_2 at

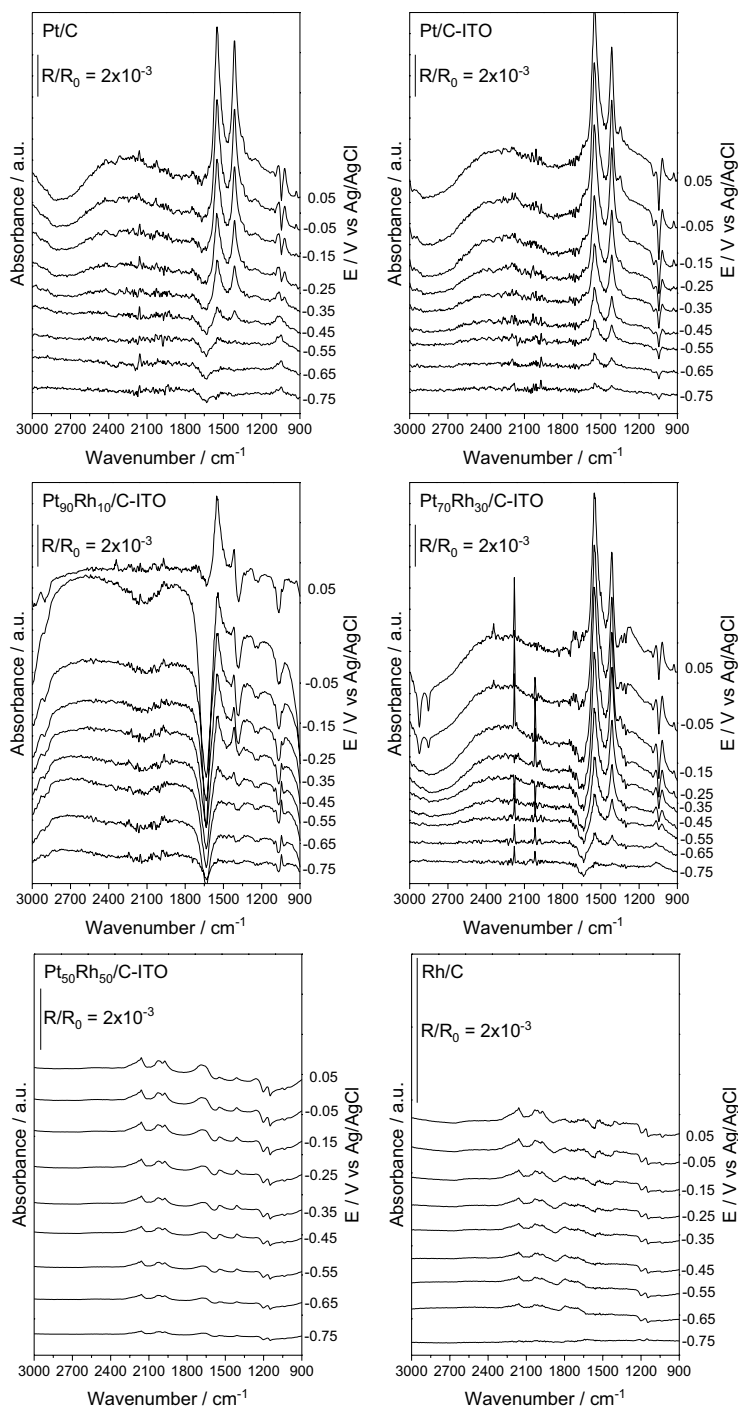


Fig. 8 In situ FTIR spectra taken at several potentials (indicated) in 1 mol L⁻¹ KOH 1.0 mol L⁻¹ ethanol for Pt/C-ITO, Rh/C-ITO and PtRh/C-ITO electrocatalysts. The backgrounds were collected at -0.85 V (Ag/AgCl)

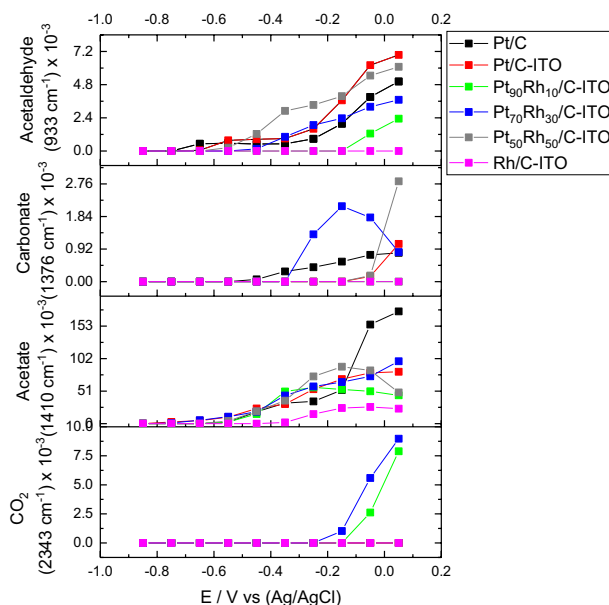


Fig. 9 Integrated CO_2 , acetate, carbonate, methyl group and acetaldehyde band intensity as a function of the electrode potential for Pt/C, Pt/C-ITO Rh/C-ITO and PtRh/C-ITO electrocatalysts (black—Pt/C; red—Pt/C-ITO; green—Pt₉₀Rh₁₀/C-ITO; blue—Pt₇₀Rh₃₀/C-ITO; gray—Pt₅₀Rh₅₀/C-ITO; and magenta—Rh/C-ITO). (Color figure online)

–0.2 V; therefore, PtRh/C-ITO (90:10) could be considered the most active electrocatalysts in EOR experiments at room temperature, since for Pt₇₀Rh₃₀/C-ITO the production of carbonate ions was observed. The presence of carbonate ions may cause, in room temperature and under these experiment conditions, a physical barrier that can reduce the catalyst ability to adsorb or oxidize alcohol on its catalytic sites.

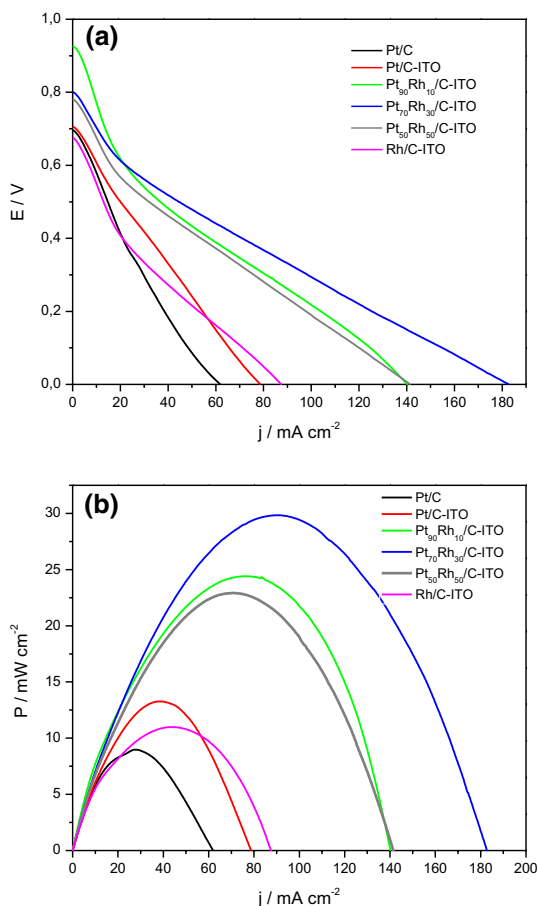
Rh/C-ITO was active for ethanol oxidation, but only acetate was observed indicating that this metal was not completely selective to C–C broken in alkaline electrolytes. The formation of acetaldehyde also confirms that part of the reaction occurred without C–C broken in alkaline electrolytes.

In accordance with our work, Zhu et al. [1] showed that a Pt₁Rh₁/RGO at 0.40 V was about 16.2 times more active in comparison with commercial Pt/C, where the superior activity was attributed to the enhanced CO_2 production generated from alcoholic groups. Zhu et al. [1] also showed the formation of $^*\text{CH}_2\text{CO}$ as intermediate, where $^*\text{CH}_2\text{CO}$ was considered as the key intermediate for C–C bond cleavage and further oxidation to form CO_2 . They concluded that Rh sites on PtRh surface can accelerate the C–C bond cleavage and also provide OH_{ad} species at low potential to oxidized intermediates adsorbed on neighboring Pt sites by bifunctional mechanism.

A single cell of a direct alkaline ethanol fuel cell operating with the prepared Pt/C, Pt/C-ITO, Pt₉₀Rh₁₀/C-ITO, Pt₇₀Rh₃₀/C-ITO, Pt₅₀Rh₅₀/C-ITO and Rh/C-ITO electrocatalysts was utilized as anode and Pt/C Basf as cathode. Test

results are illustrated in Fig. 10. All PtRh/C-ITO were more active than Pt/C confirming the beneficial effect of both Rh addition to Pt and ITO addition to carbon. Pt/C-ITO was more effective than Pt/C, which confirms the beneficial effect of ITO in the carbon. Rh/C-ITO was more effective than Pt/C, also confirming the activity of Rh in alkaline electrolytes; therefore, the rhodium could be disabled in operating conditions of direct alkaline ethanol fuel cell in long times. Pt70Rh30/C-ITO showed the highest value of maximum power density, while Pt90Rh10/C-ITO showed a highest open circuit voltage, and therefore, these electrocatalysts were considered more effective for operating in real conditions. The best activity could be related to bifunctional mechanism observed by XPS and voltammetry results, electronic effects observed by XRD results and synergism between Pt, Rh and C-ITO support.

Fig. 10 Polarization curves **a**, power density curves **b** at 80 °C of a 5 cm² in direct alkaline ethanol fuel cell using Pt/C, Pt/C-ITO, PtRh/C-ITO and Rh/C-ITO electrocatalysts used as anodes with 1 mg Pt cm⁻² catalyst loading and Pt/C BASF electrocatalyst cathode with 1 mg Pt cm⁻² catalyst loading with 20 wt% Pt loading on carbon, Nafion[®] 117 membrane treated with KOH, 1.0 mol L⁻¹ KOH + 2.0 mol L⁻¹ ethanol was used as a fuel



Conclusions

PtRh/C–ITO electrocatalysts, prepared with sodium borohydride as reducing agent, showed the presence of face cubic-centered phase and presence of oxides of indium doped with tin. All PtRh/C–ITO showed a shift to higher 2θ values compared to Pt/C electrocatalyst, indicating a formation of PtRh alloys which causes an electronic effect on the platinum.

The XPS results for Pt90Rh10/C–ITO showed the highest intensity of Pt4f; therefore, the presence of Pt active sites is the largest when compared to the other electrocatalysts. Also, the presence of oxide states in the surface for all the electrocatalysts can also support the argument of bifunctional mechanism through this paper.

Pt90Rh10/C–ITO was more active in electrochemical studies in comparison with other electrocatalysts prepared, where these results could be explained by the higher observed quantities of produced CO₂ by ATR-FTIR experiments, indicating a greater selectivity of this electrocatalyst for breaking the C–C bond.

Experiments in direct alkaline ethanol fuel cells showed that the power density values obtained for Pt70Rh30/C–ITO and Pt90Rh10/C–ITO were higher than Pt/C, where those behaviors could be related to the combination of the bifunctional mechanism, the electronic effect or to the synergetic interaction between Pt, Rh and C–ITO support.

Finally, further research is necessary to investigate PtRh/C–ITO electrocatalysts for direct alkaline ethanol fuel cells using new anionic membranes and alkaline ionomer.

Acknowledgements The authors thank FAPESP (2014/09087-4, 2014/50279-4, 2017/11937-4) and CNPq (300816/2016-2) for the financial support.

References

1. F. Zhu, K. Tu, L. Huang, X. Qu, J. Zhang, H. Liao, Z. Zhou, Y. Jiang, S. Sun, *Electrochim. Acta* **292**, 208 (2018)
2. K. Bergamaski, E.R. Gonzalez, F.C. Nart, *Electrochim. Acta* **53**, 4396e4406 (2008)
3. Y.S. Kim, S.H. Nam, H.-S. Shim, H.-J. Ahn, M. Anand, W.B. Kim, *Electrochem. Commun.* **10**, 1016e1019 (2008)
4. F. Kadirgan, S. Beyhan, T. Atilan, *Int. J. Hydrog. Energy* **34**, 4312e4320 (2009)
5. A. Kowal, S.L. Gojkovic, K.S. Lee, P. Olszewski, Y.E. Sung, *Electrochem. Commun.* **11**, 724e727 (2009)
6. T.S. Almeida, L.M. Palma, C. Morais, K.B. Kokoh, A.R. De Andrade, J. *Electrochem. Soc.* **160**, F965eF971 (2013)
7. M. Li, W.P. Zhou, N.S. Marinkovic, K. Sasaki, R.R. Adzic, *Electrochim. Acta* **104**, 454 (2013)
8. Y. Matsuura, S. Seino, T. Okazaki, T. Akita, T. Nakagawa, T.A. Yamamoto, *Rad. Phys. Chem.* **122**, 9 (2016)
9. A. Kowal, M. Li, M. Shao, K. Sasaki, M.B. Vukmirovic, J. Zhang, N.S. Marinkovic, P. Liu, A.I. Frenkel, R.R. Adzic, *Nat. Mater.* **8**, 325 (2009)
10. E.H. Fontes, R.M. Piasentin, J.M.S. Ayoub, J.C.M. da Silva, M.H.M.T. Assumpção, E.V. Spinacé, A.O. Neto, R.F.B. de Souza, *Mater. Renew. Sustain. Energy* **4**, 3 (2015)
11. E.H. Fontes, S.G. da Silva, E.V. Spinacé, A.O. Neto, R.F.B. de Souza, *Electrocatalysis* **7**, 297 (2016)

12. K. Liu, W. Wang, P. Guo, J. Ye, Y. Wang, P. Li, Z. Lyu, Y. Geng, M. Liu, S. Xie, *Adv. Funct. Mater.* **29**, 1806300 (2019)
13. S.Y. Shen, T.S. Zhao, J.B. Xu, *Int. J. Hydrog. Energy* **35**, 12911e12917 (2010)
14. P. Wang, Y. Wen, S. Yin, N. Wang, P.K. Shen, *Int. J. Hydrog. Energy* **42**, 24689e24696 (2017)
15. S. Yin, P. Wang, J. Lu, Y. Wen, L. Luo, J. Key, N. Wang, P.K. Shen, *Int. J. Hydrog. Energy* **42**, 22805e22813 (2017)
16. R.S. Henrique, R.F.B. De Souza, J.C.M. Silva, J.M.S. Ayoub, R.M. Piasentin, M. Linardi, E.V. Spinacé, M.C. Santos, A.O. Neto, *Int. J. Electrochem. Sci.* **7**, 2036 (2012)
17. J. Parrondo, R. Santhanam, F. Mijangos, B. Rambabu, *Int. J. Electrochem. Sci.* **5**, 1342 (2010)
18. E.V. Spinacé, R.R. Dias, M. Brandalise, M. Linardi, A.O. Neto, *Ionics* **16**, 16 (2010)
19. A.O. Neto, M. Linardi, D.M. dos Anjos, G. Tremiliosi-Filho, E.V. Spinace, *J. Appl. Electrochem.* **39**, 1153 (2009)
20. A.O. Neto, M. Brandalise, R.R. Dias, J.M.S. Ayoub, A.C. Silva, J.C. Penteado, M. Linardi, E.V. Spinace, *Int. J. Hydrog. Energy* **35**, 9177 (2010)
21. D. Chu, J. Wang, S. Wang, L. Zha, J. He, Y. Hou, Y. Yan, H. Lin, Z. Tian, *Catal. Commun.* **10**, 955 (2009)
22. G.L. Cordeiro, E.F. de Camargo, M.C.L. Santos, C.V. Pereira, V. Ussui, N.B. de Lima, A.O. Neto, D.R.R. Lazar, *Int. J. Electrochem. Sci.* **13**, 6388 (2018)
23. E.S.V. Neto, M.A. Gomes, G.R. Salazar-Banda, K.I.B. Eguiluz, *Int. J. Hydrog. Energy* **43**, 1788e188 (2018)
24. C.V. Pereira, E.H. Fontes, J. Nandenha, M.H.M.T. Assumpção, A.O. Neto, *Int. J. Electrochem. Sci.* **13**, 10587 (2018)
25. E.H. Fontes, C.E.D. Ramos, J. Nandenha, R.M. Piasentin, A.O. Neto, R. Landers, *Int. J. Hydrog. Energy* **44**, 937e951 (2019)
26. J.F. Moulder, J. Chastain, *Handbook of X-ray photoelectron spectroscopy: a reference book of standard spectra for identification and interpretation of XPS data* (Physical Electronics Division, Perkin-Elmer Corporation, Waltham, 1992)
27. G.S. Pawley, *J. Appl. Crystallogr.* **14**(DEC), 357 (1981)
28. M. Wojdyr, *J. Appl. Crystallogr.* **43**, 1126 (2010)
29. D.T. Clark, T. Fok, G.G. Roberts, R.W. Sykes, *Thin Solid Films* **70**(2), 261 (1980)
30. J. Bai, X. Xiao, Y.-Y. Xue, J.-X. Jiang, J.-H. Zeng, X.-F. Li, Yu. Chen, *ACS Appl. Mater. Interface* **10**, 19755 (2018)
31. L. Fang, J. He, S. Saipanya, X. Huang, *Int. J. Electrochem. Sci.* **10**, 5350 (2015)
32. X. Fang, L. Wang, P.K. Shen, G. Cui, C. Bianchini, *J. Power Sour.* **195**(5), 1375 (2010)
33. A.N. Geraldes, D.F. Da Silva, E.S. Pino, J.C.M. Da Silva, R.F.B. De Souza, P. Hammer, E.V. Spinacé, A.O. Neto, M. Linardi, M.C. Dos Santos, *Electrochim. Acta* **111**, 455 (2013)
34. Z.-Y. Zhou, Q. Wang, J.-L. Lin, N. Tian, S.-G. Sun, *Electrochim. Acta* **55**(27), 7995 (2010)

Publisher's Note Springer Nature remains neutral with regard to jurisdictional claims in published maps and institutional affiliations.